Modulational instability and charge localization in the Holstein-SSH model of DNA with mass impurities

R. Y. Ondoua [1,2,3,*] A. Dang Koko [2,3,4,†] R. Abouem A Ribama [1,‡] C. B. Tabi [2,5]
H. P. Ekobena Fouda [2,3] and J. P. Nguenang [1]

[1]*Pure Physics Laboratory: Group of Nonlinear Physics and Complex Systems, Department of Physics, University of Douala, P.O. Box 24157, Douala, Cameroon*

[2]*Laboratory of Biophysics, Department of Physics, Faculty of Science, University of Yaoundé I, P.O. Box 812, Yaoundé, Cameroon*

[3]*African Centre for Advanced Studies, P.O. Box 4477, Yaoundé, Cameroon*

[4]*Department of Maintance, Higher Technical Teachers' Training College, University of Ebolowa, P.O. Box 886, Ebolowa, Cameroon*

[5]*Botswana International University of Science and Technology, Private Mail Bag 16, Palapye, Botswana*

(Received 29 September 2025; accepted 3 February 2026; published 20 February 2026)

This research investigates the stability of localized charge modes in a Holstein-SSH DNA model incorporating a mass impurity. By deriving a semidiscrete nonlinear Schrödinger equation through Hamiltonian formalism and the adiabatic approximation, we analyze the modulational instability to assess the impact of impurity parameters on mode stability. Analytical results reveal that impurity mass significantly influences charge localization, especially near the Brillouin zone edges, with low coupling parameters favoring localized modes and higher values promoting charge delocalization. Numerical simulations confirm that the impurity's mass and sign critically affect energy and charge localization, with negative masses acting as potential wells and positive masses inducing dispersive effects. These findings highlight the crucial role of mass impurities in modulating charge transport in DNA, offering insights for designing biomolecular and nanotechnological systems with controlled electronic properties.

DOI: 10.1103/xc38-djk7

I. INTRODUCTION

Deoxyribonucleic acid (DNA) is a molecule present in all living cells [1–3]. DNA is the carrier of genetic information and its hereditary transmission, the main constituent of chromosomes [4]. In eukaryotic cells, DNA is contained in the nucleus and a small part is in the mitochondria and chloroplasts [5]. In prokaryotic cells, DNA is contained in the cytoplasm [6]. Some viruses also have DNA in their capsid [7]. DNA molecules are made up of two chains whose nucleotides are hybridized two by two along their entire length [8]. They are organized into a very original structure known as the double helix [9]. The three-dimensional (3D) version of the DNA molecule is an assembly of two helical chains (or strands) wrapped around an axis [10]. This double helix is maintained by hydrogen bonds between the bases that face each other [11]. These bases, called complementary [adenine (A) binds with thymine (T), and only with it, by establishing weak bonds (hydrogen bonds), and cytosine (C) binds with guanine (G)], form like the rungs of a ladder [12]. The two strands of DNA therefore provide the same information, like a photograph and its negative [13,14].

During cell division, DNA compacts around proteins and organizes itself into visible rods, the chromosomes [15]. Other sources, environmental or linked to human activities, can also modify DNA [16]. Errors can creep into the DNA sequence: these are mutations [17,18]. Mutations can occur during DNA replication, but most of the time they are corrected [19]. Mutagenic factors are biological, physical, or chemical [20]. Nature has developed particularly effective agents: viruses, some of which can kill [21]. X-rays, ultraviolet rays, and radioactivity are physical agents with a radical method: they break the DNA molecule [22]. It is important to note that during cell division, DNA is copied thanks to the complementarity of its bases [23]. As a result, all cells in the same organism have the same DNA molecules [24].

DNA leads to the synthesis of proteins, which are associated with very specific functions in the cell [25]. The following two steps are important: transcription, which is the production of a copy of DNA into messenger ribonucleic acid (RNA), and translation, the messenger of genetic information [26]. This message results in the synthesis of a protein [27]. The proteins thus produced by the body play various physiological roles: a structural role (cell membranes, etc.), biosynthesis of molecules essential to life (carbohydrates, lipids, nucleic acids), the role of messengers (hormones), etc. [28]. Proteins are therefore major constituents and the main cell builders [29].

*Contact author: yanickondouar@yahoo.com
†Contact author: dangadamou@gmail.com
‡Contact author: ribamarodrigue@gmail.com

Published by the American Physical Society under the terms of the Creative Commons Attribution 4.0 International license. Further distribution of this work must maintain attribution to the author(s) and the published article's title, journal citation, and DOI.

Like any biological molecule, DNA is also subject to mass impurities [30]. A mass impurity in DNA refers to contamination of the DNA sample by other molecules, such as proteins or RNA, whose molecular mass is different from that of pure DNA [31]. These include proteins that can contaminate DNA during the extraction steps, particularly histones and nonhistone proteins that associate with DNA to form chromatin [32]. Then RNA molecules can also be present in the DNA sample, either by coextraction or by degradation of the DNA itself into smaller components [33]. Finally, other contaminants—depending on the extraction methods and the type of sample—such as salts, solvents, or other cellular debris, may be present [34].

Mass impurities in a DNA sample can distort quantification, interfere with downstream analyses, and lead to erroneous results, thus compromising the reliability of genetic studies, disease diagnosis, and forensic applications such as identification [35,36]. DNA purity is therefore essential to ensure the accuracy of analyses and conclusions [37]. This purification separates DNA from cellular impurities using physical and chemical properties such as mass [35].

DNA itself is negatively charged due to the phosphate groups in its backbone, which affects its interaction with other molecules and electric fields, while impurities (proteins, cellular debris) are removed through precipitation, centrifugation, or extraction steps that exploit differences in mass and solubility [38]. Furthermore, charge transport in DNA refers to two concepts: the movement of the DNA itself in response to an electric field and the transport of electric charges through the DNA molecule [39]. DNA can be moved toward a positive charge using techniques such as gel electrophoresis [40]. Research is being done to investigate the ability of DNA to conduct charges, which could have applications in molecular electronics [41]. Indeed, the idea that double-stranded DNA, the carrier of genetic information in most living organisms, could serve as a channel for the rapid transport of electrons along the axis of its base pair stack was first revealed in 1962 by Eley and Spivey [42]. Since then, research has been carried out on conductivity in DNA, based on these pioneers [43–46]. It has been proven that charge conduction occurs through overlapping base orbitals along the double helix [47–50]. These studies suggest that double-stranded DNA could exhibit "wirelike" behavior [51,52]. Further work on the phenomenon of modulational instability (MI) has been carried out to highlight the activity of charge and energy transport in DNA and in certain biological molecules [53–57].

Several biophysical models describing charge transport in DNA have been studied over the years, including the Holstein–Su-Schrieffer-Heeger Hamiltonian model, whose dynamics leads to a nonlinear Schrödinger equation [58,59]. This equation finds its applications in several fields, in hydrodynamics, acoustics, Bose Einstein condensates, optical fiber, and biophysics, to name but a few [60–66]. The analytical and numerical resolution of the nonlinear Schrödinger equation, discrete or continuous, often induces the propagation of solitary waves in biological macromolecules such as DNA [67–70].

It has been experimentally proven that proteins, by binding to DNA, can modulate long-range charge transport, both positively and negatively. Indeed, given the sensitivity of this chemistry to base pair stacking, DNA charge transport is exploited as a sensor of perturbations in this stacking [71]. Furthermore, it is proven that a certain defect located at the end of the DNA molecule has a considerable effect on the charge transport properties [72]. Indeed, the dynamics of interactions in DNA described above also includes the propagation of breathers [73,74]. To model these phenomena, the theory uses various biophysical models. Among the most studied, the Holstein–Su-Schrieffer-Heeger (HSSH) model incorporates electron-phonon interactions to describe the dynamics of charge transport within the framework of a nonlinear Schrödinger equation. This equation offers solutions in the form of localized waves called solitons or "breathers," where the energy is confined spatially and oscillates temporally, playing a key role in the stability and efficiency of charge transport. Such solutions illustrate the nonlinear and quantum nature of the phenomenon, and open the way to a better understanding of the energy function of DNA.

In nonlinear dynamics, a breather is a special type of nonlinear wave where energy is localized in space and oscillates in time [75–78]. The presence of an impurity causes the formation of structural defects in DNA. These defects have a major impact on charge transport, as they can disrupt the continuity of the conductive path, leading to interruptions or slowdowns in the propagation of electrical or electronic charges. Such an alteration can have significant biological consequences, notably by disrupting the mechanisms that recognize damaged DNA by repair enzymes, or by affecting the stability and regulation of gene expression. In our study, we aim to deepen our knowledge of this topic by examining the influence of mass-type impurities on charge transport in DNA.

This paper is structured as follows. In the next section, titled "Model," we derive the discrete nonlinear Schrödinger equation through Hamilton's equations, after introducing an impurity mass around the central site n. In Sec. III, titled "Modulational instability," we conduct a linear stability study of this equation describing the charge transport dynamics in DNA in the presence of a mass impurity. Then, in Sec. IV, titled "Breathers and energy," the multiscale method is used to transform the equation of motion into a continuous nonlinear Schrödinger equation. The equation is then solved, and breather solutions and impurity modes are determined and analyzed. The last section presents the conclusions.

II. MODEL

In this section, we consider the Holstein–Su-Schrieffer-Heeger (HSSH) model as described in Ref. [58] by the Hamiltonian:

$$H = H_{\text{lat}} + H_{\text{el}} + H_{\text{int}}. \tag{1}$$

In Eq. (1), H_{lat} describes the transversal oscillations of the base pairs and is defined as

$$H_{\text{lat}} = \sum_n \frac{M}{2}\left(\frac{du_n}{dt}\right)^2 + \frac{K}{2}u_n^2. \tag{2}$$

u_n is the stretching of the hydrogen bonds of the nth base pair from the equilibrium position and K stands for the elastic

constant of the strands. In Eq. (2), M is considered as the effective mass of the base pair. To better study charge transport in DNA, in the present work we introduce a mass impurity around the central site n in a base pair. The latter will be used, later, in the form

$$M = m_0(1 + \Delta m \delta_{n,0}). \tag{3}$$

m_0 is the initial mass, Δm is a parameter which measures the magnitude of inhomogeneity in the base pair of DNA, and $\delta_{n,0}$ is the Dirac's function. Δm belongs in the interval $]-1, +\infty[$ as defined in Ref. [79].

$H_{\rm el}$ is the electronic part of the Hamiltonian given by

$$H_{\rm lat} = \sum_n \nu_{n,n+1}(a_n^\dagger a_{n+1} + a_{n+1}^\dagger a_n), \tag{4}$$

where $a_n^\dagger(a_n)$ are, respectively, the charge creation and annihilation operator at the site n. $\nu_{n,j}$ describes the matrix elements of the charge tranfer from the nth site to the jth site.

The last term in Eq. (1), $H_{\rm int}$ describes the coupling between the charge and lattice vibrations,

$$H_{\rm int} = \sum_n \alpha' u_n a_n^\dagger a_n, \tag{5}$$

with α' the charge vibration coupling parameter. In the classical Su-Schrieffer-Heeger model, the matrix elements $\nu_{n,n+1}$ are constant. In this work, they can be combined to the relative charge displacement along the stack, $L_{n+1} - L_n$, where we introduce an effective coupling constant. Therefore, $\nu_{n,n+1}$ can be written as

$$\nu_{n,n+1} = \nu^0_{n,n+1} + \nu'_{n,n+1}(L_{n+1} - L_n). \tag{6}$$

$\nu^0_{n,n+1}$ is the transfer integral between π orbitals between adjacent base pairs. This introduces, therefore, the Hamiltonian:

$$H_{\rm long} = \sum_n \frac{M}{2}\left(\frac{dL_n}{dt}\right)^2 + \frac{I}{2}(L_{n+1} - L_n)^2. \tag{7}$$

$H_{\rm long}$ models longitudinal or internal vibrations of base pairs and I is the longitudinal coupling constant.

Applying Hamilton's equations and considering φ_n the charge density probability, we obtain the following set of equations:

$$i\hbar\frac{d}{dt}\varphi_n(t) = [\nu^0 + \nu'(L_{n+1} - L_n)]\varphi_{n+1} \times [\nu^0 + \nu'(L_n - L_{n-1})]\varphi_{n-1} + \alpha' u_n \varphi_n, \tag{8a}$$

$$M\frac{d^2}{dt^2}u_n(t) = -Ku_n - \alpha'|\varphi_n|^2, \tag{8b}$$

$$M\frac{d^2}{dt^2}L_n(t) = I(L_{n+1} + L_{n-1} - 2L_n) + \nu'(\varphi^*_{n+1}\varphi_n + \varphi^*_n\varphi_{n+1}) - \nu'(\varphi^*_{n-1}\varphi_n + \varphi^*_n\varphi_{n-1}). \tag{8c}$$

We have made the following transformations: $\nu^0_{n,n+1} = \nu^0_{n,n-1} = \nu^0$ and $\nu'_{n,n+1} = \nu'_{n,n-1} = \nu'$, ν' being the effective coupling parameter, while I is the longitudinal coupling constant. ν^0 is a constant that describes the nearest-neighbor transfer integral between adjacent base pairs.

For the following, we apply the adiabatic approximation to Eq. (8b) and consider in Eq. (8c) a charge propagating with speed v_1 and define the wave variable $\xi = x - v_1 t$. Also,

$$\frac{\partial^2}{\partial \xi^2}L_n(t) \equiv \frac{(L_{n+1} + L_{n-1} - 2L_n)}{\epsilon^2}, \tag{9}$$

knowing that $x = n\epsilon$, with ϵ the lattice parameter [80]. Using Eq. (9) in Eq. (8b) with the help of Eq. (8a), we derive a modified discrete nonlinear Schrödinger (MDNLS) equation:

$$i\hbar\dot{\varphi}_n = -\frac{(\alpha')^2}{K}|\varphi_n|^2\varphi_n + \nu^0(\varphi_{n+1} + \varphi_{n-1}) - \frac{(\nu')^2\epsilon^2}{I\epsilon^2 - Mv_1^2}(\varphi^*_n\varphi_{n+1} + \varphi_n\varphi^*_{n+1})\varphi_{n+1} - \frac{(\nu')^2\epsilon^2}{I\epsilon^2 - Mv_1^2}(\varphi^*_n\varphi_{n-1} + \varphi_n\varphi^*_{n-1})\varphi_{n-1}. \tag{10}$$

Some numerical values of the parameters used in this work are as follows:

$\alpha' = 0.13\,\text{eV Å}^{-1}$, $\nu^0 = 0.084\,\text{eV}$, $\nu' = 0.4\,\text{eV Å}^{-1}$, $K = 0.855\,\text{eV Å}^{-2}$, and $I = 0.062\,\text{eV Å}^{-2}$ [59]. The time unit (t.u.) adopted here is 1 t.u. $= 1.0214 \times 10^{-13}$ s.

Now let us take the solution of Eq. (10) in the form

$$\varphi_n = \varphi_0 e^{i(kna - \omega t)}. \tag{11}$$

The insertion of Eq. (11) into Eq. (10) gives

$$i\dot{\varphi}_n + Q_1[\varphi_{n-1} + \varphi_{n+1}] + Q_2|\varphi_n|^2\varphi_n - \frac{Q_3}{m_0(1 + \Delta m\delta_{n,0})v_1^2 - I\epsilon^2}|\varphi_n|^2\varphi_n = 0. \tag{12}$$

$Q_1 = \frac{-\nu^0}{\hbar}$, $Q_2 = \frac{(\alpha')^2}{\hbar K}$, and $Q_3 = \frac{[2+2\cos(2k)](\nu')^2\epsilon^2}{\hbar}$. Equation (12) is a discrete nonlinear Schrödinger equation that describes charge transport in DNA in the presence of a mass impurity around the central site $n = 0$; in other words $\delta_{n,0} = \delta_{0,0}$. Analysis of the nonlinearity coefficient of Eq. (12) shows the presence of mass and longitudinal couplings. Mass coupling aims to promote collective dynamics, given that the speed and nature of oscillations (or vibrations) are influenced by the total mass. Mass coupling can thus slow down or restrict the propagation of certain waves or deformations. However, longitudinal coupling contributes to the efficient transmission of deformations or vibrations along the DNA axis, facilitating the propagation of mechanical signals or solitary waves. Their use in the same model implies that these two effects can cancel each other out or reduce each other's contributions, depending on their relative strength. Specifically, strong mass coupling can limit effective longitudinal propagation, while strong longitudinal coupling can counteract the mass effect by promoting rapid vertical transmission. It is therefore essential to take these antagonistic effects into account in order to obtain accurate predictions on the dynamic behavior of DNA.

III. MODULATIONAL INSTABILITY

In this section, we conduct a study of the linear stability of charge transport dynamics under the effect of mass impurity in DNA through the phenomenon of modulational instability. For this, let us take the solution of Eq. (12) in the form of a

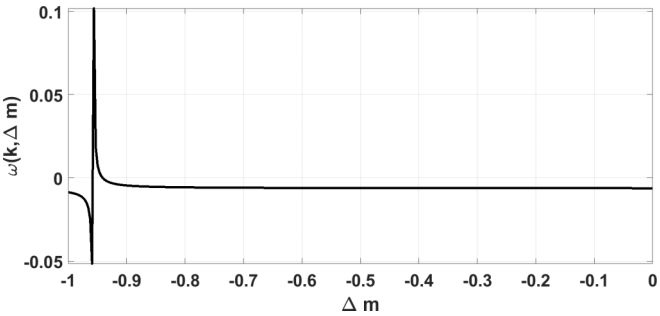


FIG. 1. Plot of modulational instability dispersion relationship $\omega(k, \Delta m)$ as a function of mass impurity Δm for $k = 0.45\pi$. The other parameters are $\alpha' = 0.13\,\text{eV Å}^{-1}$, $\nu^0 = 0.025\,\text{eV}$, $\nu' = 0.4\,\text{eV Å}^{-1}$, $K = 0.855\,\text{eV Å}^{-2}$, $I = 0.062\,\text{eV Å}^{-2}$, $m_0 = 1$, $v_1 = 1.2$, $\delta_{0,0} = 1$, and $a = 1$.

plane wave [81–83]:

$$\varphi_n = \varphi_0 e^{i(kn-\omega t)}. \tag{13}$$

The insertion of Eq. (13) into Eq. (12) gives the resultant dispersion relationship:

$$\omega = \left(\frac{Q_3}{m_0(1+\Delta m\delta_{0,0})v_1^2 - I\epsilon^2} - Q_2\right)|\varphi_0|^2 - 2Q_1\cos(k). \tag{14}$$

The dispersion relation given by Eq. (14) has been plotted in Fig. 1.

This figure shows the existence of a mass defect value Δm around -0.95 at which the dynamics of the localized impurity mode could be unstable. This shows that the impurity significantly alters the dispersion relationship and that there is a localized impurity mode that stands out from the main spectrum. This observation suggests that introducing an impurity at this specific value can induce instability in DNA dynamics, potentially affecting breather localization and stability. Furthermore, a more in-depth study of this critical area would allow for a better understanding of the interaction between the mass defect and the behavior of the localized impurity mode.

Let us perturb the solution in amplitude; we have

$$\varphi_n = (\varphi_0 + c_n)\exp[i(kn - \omega t)]. \tag{15}$$

The introduction of Eq. (15) into Eq. (12) gives the following perturbation evolution equation:

$$\begin{aligned} i\dot{c}_n &+ Q_1\cos(k)(c_{n+1} + c_{n-1} - 2c_n) \\ &+ Q_1 i\sin(k)(c_{n+1} - c_{n-1}) + \varepsilon_0(c_n + c_n^*) = 0, \end{aligned} \tag{16}$$

with $\varepsilon_0 = (Q_2 - \frac{Q_3}{m_0(1+\Delta m\delta_{0,0})v_1^2 - I\epsilon^2})|\varphi_0|^2$. Solution of Eq. (16) is taken in the form

$c_n(t) = a_1\exp[i(Qn - \Omega t)] + a_2^*\exp[-i(Qn - \Omega^* t)]$, Q and Ω being unstable wave number and the frequency of modulation, respectively. The following linear homogeneous system of Eq. (16), for unknowns a_1 and a_2^* complex variables, reveals a nontrivial solution if the determinant of its matrix dissolves

$$\begin{bmatrix} \varpi + A_{11} & \varepsilon_0 \\ \varepsilon_0 & -\varpi + A_{11} \end{bmatrix}\begin{bmatrix} a_1 \\ a_2^* \end{bmatrix} = \begin{bmatrix} 0 \\ 0 \end{bmatrix}, \tag{17}$$

with $\varpi = \Omega - 2Q_1\sin(k)\sin(Q)$, $A_{11} = 2Q_1\cos(k)(\cos(Q) - 1) + \varepsilon_0$. Hence the following relationship is obtained:

$$\varpi^2 = 16Q_1\cos(k)\sin^2\left(\frac{Q}{2}\right)\left[Q_1\cos(k)\sin^2\left(\frac{Q}{2}\right) - \frac{\varepsilon_0}{2}\right]. \tag{18}$$

If ϖ^2 is negative, two complex numbers are solutions of the above equation and the exponential growth takes place with rate $\Gamma(k, Q) = \sqrt{-\varpi^2}$. This is possible if the initial amplitude $|c_0|$ exceeds the threshold amplitude $|\varphi_{0,cr}|$ defined as follows:

$$|\varphi_0|^2 \geqslant |\varphi_{0,cr}|^2 = \frac{2Q_1\cos(k)\sin^2\left(\frac{Q}{2}\right)}{Q_2 + Q_3/\left[m_0(1+\Delta m\delta_{0,0})v_1^2 - I\epsilon^2\right]}. \tag{19}$$

Figure 2 shows the evolution of the modulational instability gain $\Gamma(k, Q)$ as a function of the mass impurity Δm for different fixed values of the wave number k. For each value of k, the gain $\Gamma(k, Q)$ varies significantly with Δm, which represents the local mass variation at the central site of the DNA network. Indeed, for $k = 0.15\pi$ [Fig. 2(a)], the variation of the gain as a function of Δm is relatively stable; there appears around the value of $\Delta m = -0.95$ a zone of instability. When $k = 0.35\pi$ [Fig. 2(b)], we observe a more marked variation with a zone where the gain decreases, highlighting a sensitivity to the variation of the parameter k. This is confirmed when for $k = 0.45\pi$ and $k = 0.48\pi$ [Figs. 2(c) and 2(d)], the amplitude of the gain decreases; in addition the latter presents sharper maxima and variations indicating the influence of Δm on the gain, which indicates that the charge carrier modes are more likely to be modulated or destabilized by a local impurity with a critical value $\Delta m = -0.95$.

This result shows that, for some modes whose wave number is close to the limit of the first Brillouin zone, the impure mass effect Δm plays a more critical role on the dynamics of the carrier modes. Moreover, the gain behavior differs depending on the values of Δm.

Indeed, the Δm axis extends from negative values close to -1 to positive values. We observed that the gain behavior varies depending on the impurity mass. In particular, it differs when the mass is lower (light impurity) or higher (heavy impurity) than the normal mass. An asymmetry can appear, showing that the type of impurity (light or heavy) influences the dynamics of the system differently. Figure 2 demonstrates that the modified local mass (impure mass) in a DNA base acts as a powerful regulator of the stability of charge waves. Carrier modes with wave numbers close to 0.45π–0.48π are particularly sensitive to this impurity, which may indicate critical points for the manipulation or understanding of charge transport in biological macromolecules. This sensitivity strongly depends on the sign and magnitude of the mass impurity Δm.

Figure 3 plots the modulational instability gain $\Gamma(k, Q)$ as a function of the unstable wave number Q for a fixed value of $k = 0.45\pi$. A positive value of Γ indicates modulatory instability; i.e., small amplitude perturbations with wave number Q grow in time, leading to the formation of localized structures (breathers, solitons). This bell shape is centered

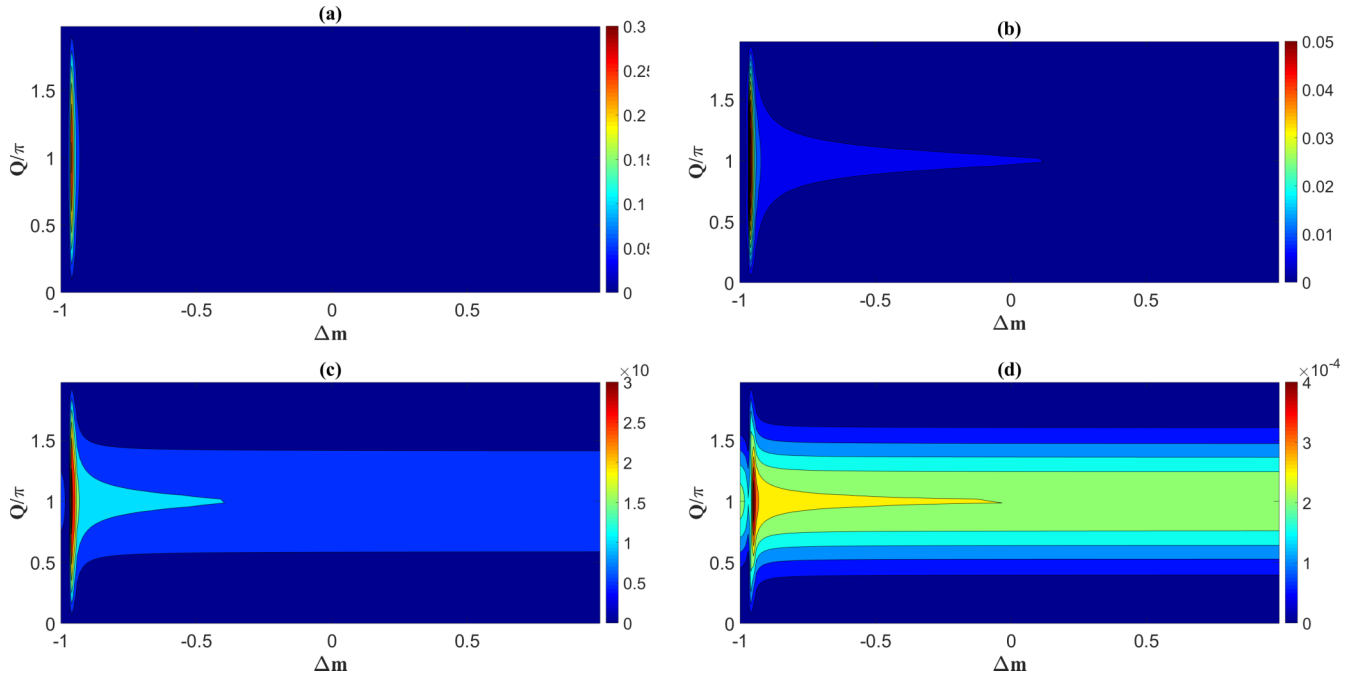


FIG. 2. Plot of modulational instability gain $\Gamma(k, Q)$ as a function of mass impurity Δm. (a): $k = 0.15\pi$; (b): $k = 0.35\pi$; (c): $k = 0.45\pi$; (d): $k = 0.48\pi$. The other parameters are $\alpha' = 0.13\,\text{eV Å}^{-1}$, $\nu^0 = 0.025\,\text{eV}$, $\nu' = 0.4\,\text{eV Å}^{-1}$, $K = 0.855\,\text{eV Å}^{-2}$, $I = 0.062\,\text{eV Å}^{-2}$, $m_0 = 1$, $v_1 = 1.2$, $\delta_{0,0} = 1$, and $a = 1$.

around certain values of Q, where the gain is maximal. This means that certain perturbations of a specific wavelength are preferentially amplified under the influence of the mass defect Δm.

Figure 4 analyzes the impact of varying the parameter ν^0, representing the integral transfer between neighboring sites in the Holstein-SSH model, on the modulational instability gain $\Gamma(k, Q)$ as a function of the mass impurity Δm. Two extreme values of ν^0 are compared: (a): $\nu^0 = 0.005\,\text{eV}$, corresponding to a weak transfer between sites, and (b): $\nu^0 = 0.5\,\text{eV}$, representing a stronger transfer. The other model parameters remain constant. When ν^0 is very small [Fig. 4(a)], the instability gain $\Gamma(k, Q)$ is globally small and insensitive to Δm, indicating that the system dynamics is little affected by impurities when the charge is highly localized. On the other hand, for a high value of ν^0 [Fig. 4(b)], the system becomes much more sensitive to Δm, with significant variations in the instability gain, illustrating a stronger reaction of the charge to the presence of a local disturbed mass, with the appearance of sharp peaks indicating increased instability and possible charge localizations.

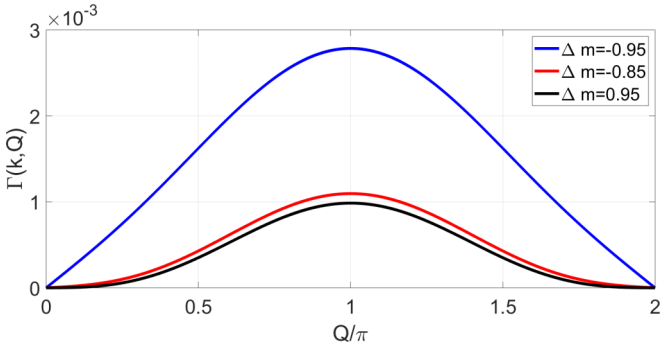


FIG. 3. Plot of modulational instability gain $\Gamma(k, Q)$ as a function of the unstable wave number Q for $k = 0.45\pi$. The other parameters are $\alpha' = 0.13\,\text{eV Å}^{-1}$, $\nu^0 = 0.025\,\text{eV}$, $\nu' = 0.4\,\text{eV Å}^{-1}$, $K = 0.855\,\text{eV Å}^{-2}$, $I = 0.062\,\text{eV Å}^{-2}$, $m_0 = 1$, $v_1 = 1.2$, $\delta_{0,0} = 1$, and $a = 1$.

Physically, ν^0 controls how easily charge moves between sites: for low values, the charge is essentially localized, limiting the effect of impurities, while for high values, the charge can move more freely, making the impurity a center of perturbation strongly influencing the stability of propagation modes. This has important implications for transport in DNA, showing that strong interactions between sites combined with local defects can significantly modify the stability of charge transport and energy localization.

On the other hand, Fig. 5 provides an in-depth analysis of the evolution of the modulational instability gain $\Gamma(k, Q)$ as a function of the mass impurity Δm, by comparing two values of the effective coupling parameter ν': (a) $\nu' = 0.04\,\text{eV Å}^{-1}$ and (b) $\nu' = 1.4\,\text{eV Å}^{-1}$, while keeping the other model parameters constant. The parameter ν' represents the strength of the coupling between electronic dynamics and lattice vibrations, depending on the relative displacement of charges between sites. When it is low ($\nu' = 0.04$) [Fig. 5(a)], the Γ curve remains relatively flat, indicating a low sensitivity of the system to the mass impurity, which only marginally affects the charge stability. In contrast, for a stronger coupling ($\nu' = 1.4$) [Fig. 5(b)], the stability becomes very sensitive to Δm, with marked variations of Γ potentially leading to increased instability or the formation of localized states, such as impure modes or breathers. Thus this analysis shows that the impact of a mass impurity on the system dynamics is

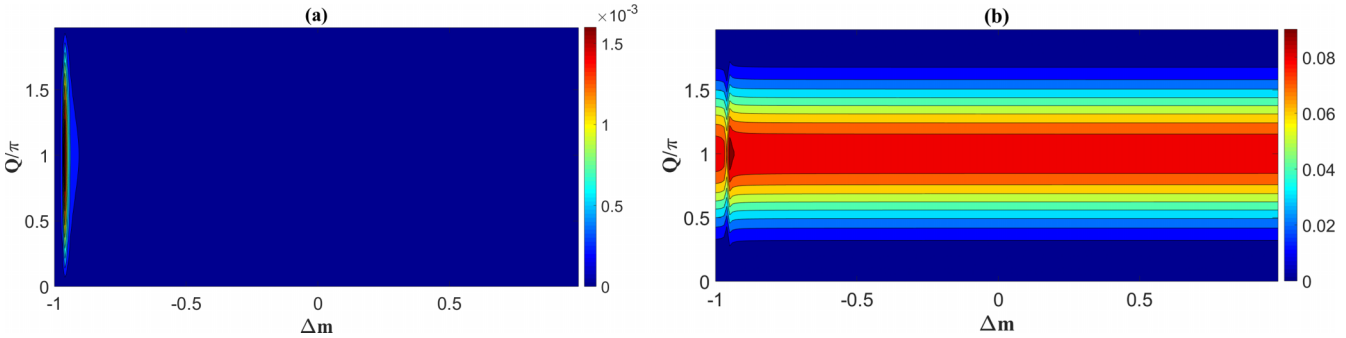


FIG. 4. Plot of modulational instability gain $\Gamma(k, Q)$ as a function of mass impurity Δm. (a) $\nu^0 = 0.005\,\text{eV}$; (b) $\nu^0 = 0.5\,\text{eV}$. The other parameters are $\alpha' = 0.13\,\text{eV Å}^{-1}$, $\nu' = 0.4\,\text{eV Å}^{-1}$, $K = 0.855\,\text{eV Å}^{-2}$, $I = 0.062\,\text{eV Å}^{-2}$, $m_0 = 1$, $v_1 = 1.2$, $\delta_{0,0} = 1$, and $a = 1$.

strongly modulated by the strength of the electron-phonon coupling: a strong coupling makes the structure more vulnerable to local defects, which can influence the charge transfer in DNA, especially in contexts where mutations or chemical modifications modify the local mass. In sum, Fig. 5 highlights that the parameter ν' plays a crucial role in the sensitivity of the system to impurities, highlighting the complexity of the interaction mechanisms in biological or nanotechnological systems modeled by this framework.

We note that both Figs. 4 and 5 provide an analysis of the sensitivity of the modulational instability gain $\Gamma(k, Q)$ to the presence of impurities, but they differ in the parameters they highlight and in their physical significance. Figure 4 studies the effect of the parameter ν_0, representing the full transfer between sites in the Holstein-SSH model, by comparing a low transfer ($\nu_0 = 0.005\,\text{eV}$) to a high transfer ($\nu_0 = 0.5\,\text{eV}$), while keeping the other parameters constant. It shows that when ν_0 is low, the system is not very sensitive to impurities, with an overall low and little variable instability gain, indicating a strongly localized charge little affected by defects. On the other hand, for a high ν_0, the sensitivity increases significantly, with notable variations in the Γ, reflecting a stronger reaction of the system dynamics to impurities, notably through the appearance of instability peaks. Figure 5, for its part, explores the effect of the parameter ν', representing the coupling dependent on the relative displacement of the charges, by comparing a weak coupling ($\nu' = 0.04\,\text{eV Å}^{-1}$) with a strong coupling ($\nu' = 1.4\,\text{eV Å}^{-1}$). It demonstrates that when ν' is small, the stability of the system is little affected by Δm, with minimal variation in the gain, while stronger coupling considerably amplifies the sensitivity, making the stability very dependent on the impurity, with large fluctuations. In summary, Fig. 4 highlights that the intersite transfer capacity (ν_0) moderates the overall sensitivity of the system to impurities, ranging from little affected dynamics to a strong response to defects. Figure 5 shows that the electron-phonon coupling strength (ν') is a determining factor that can transform low sensitivity into increased instability, highlighting that the strength of the local interaction plays a crucial role in the system response to impurities. Together, these figures illustrate that the stability of charge transport in the model depends on both the intersite transfer strength and the dynamic coupling strength, with amplified effects when these parameters are high.

Figure 6 further analyzes the modulatory instability gain $\Gamma(k, Q)$ as a function of the disturbing wave number Q, fixed at $k = 0.45\pi$, with an impurity of mass $\Delta m = -0.95$. Two scenarios are compared: (a) for an effective coupling $\nu' = 0.4\,\text{eV Å}^{-1}$, where the instability is more pronounced, and (b) for an intersite transfer $\nu^0 = 0.025\,\text{eV}$, which limits the perturbation growth band. The gain $\Gamma(k, Q)$ shows a peak at a particular value of Q, indicating the presence of a most unstable mode likely to favor the formation of localized structures like breathers, with little or no gain for very low or high Q, in accordance with the theory of modulational instability. The variation of ν' influences the strength of the intersite coupling, strengthening or weakening the amplitude of the instability, while the value of ν^0 modifies the width and height of the gain

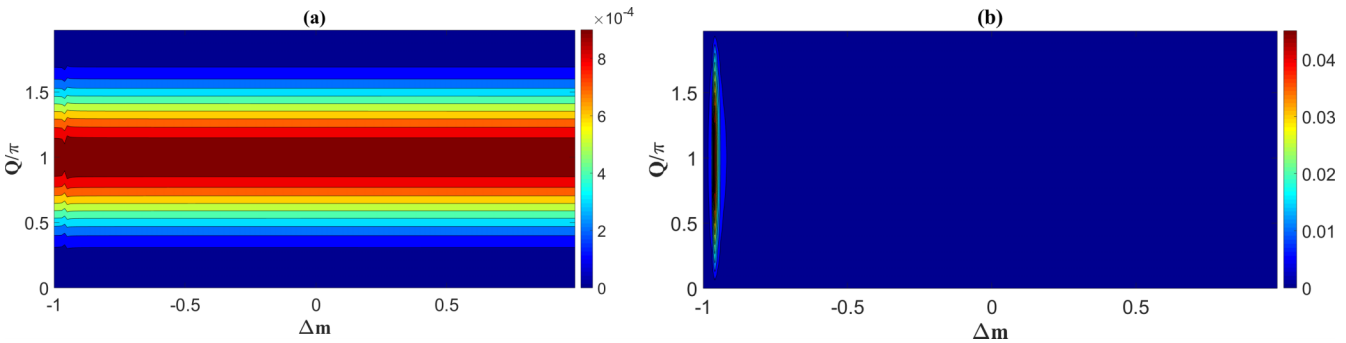


FIG. 5. Plot of modulational instability gain $\Gamma(k, Q)$ as a function of mass impurity Δm. (a) $\nu' = 0.04\,\text{eV Å}^{-1}$; (b) $\nu' = 1.4\,\text{eV Å}^{-1}$. The other parameters are $\alpha' = 0.13\,\text{eV Å}^{-1}$, $\nu^0 = 0.025\,\text{eV}$, $K = 0.855\,\text{eV Å}^{-2}$, $I = 0.062\,\text{eV Å}^{-2}$, $m_0 = 1$, $v_1 = 1.2$, $\delta_{0,0} = 1$, and $a = 1$.

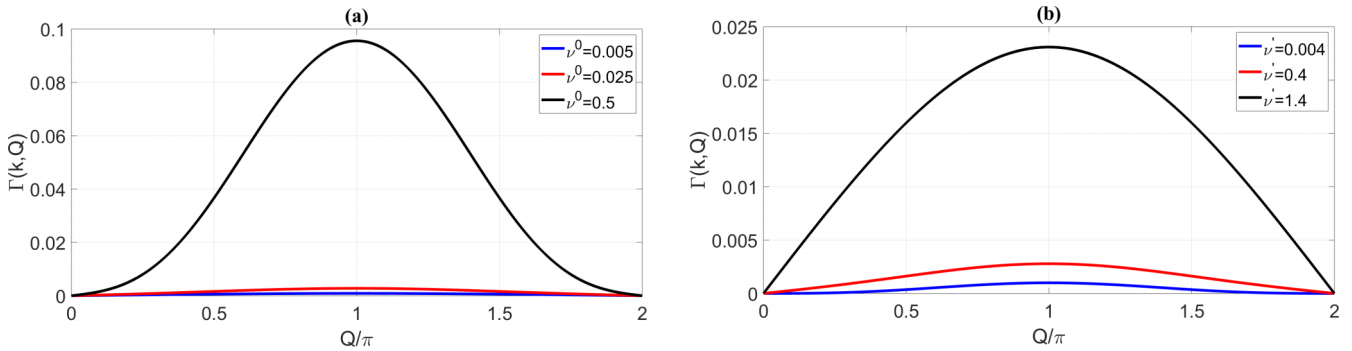


FIG. 6. Plot of modulational instability gain $\Gamma(k, Q)$ as a function of the unstable wave number Q for $k = 0.45\pi$ and $\Delta m = -0.95$. (a) $\nu' = 0.4\,\text{eV Å}^{-1}$; (b) $\nu^0 = 0.025\,\text{eV}$. The other parameters are $\alpha' = 0.13\,\text{eV Å}^{-1}$, $K = 0.855\,\text{eV Å}^{-2}$, $I = 0.062\,\text{eV Å}^{-2}$, $m_0 = 1$ $v_1 = 1.2$, $\delta_{0,0} = 1$, and $a = 1$.

peak, affecting the stability or instability band. The negative mass impurity, close to -1, acts as a local defect modifying the dispersion and interaction, favoring the growth of some perturbations. In summary, this figure shows that the charge dynamics in the Holstein-SSH model, strongly influenced by a local impurity, exhibits a selective modulatory instability in Q, whose manifestation is strongly dependent on the coupling parameters ν' and ν^0, which regulate the transmission and dynamics of charges at the discrete network scale.

IV. BREATHERS AND ENERGY

A. Continuum nonlinear Schrödinger equation

We apply a semidiscrete multiple-scale method to investigate discrete breathers, the average number of the charge density, and we analyze their behavior. For this end, we are now seeking a modulated solution to Eq. (12) in the form of

$$\varphi_n = \varepsilon\varphi_n, \tag{20}$$

where ε is a small positive real number representing the relative amplitude of the charge density. Consequently, Eq. (12) simplifies to

$$i\dot{\varphi}_n + Q_1[\varphi_{n-1} + \varphi_{n+1}] + Q_2'\epsilon^2|\varphi_n|^2\varphi_n = 0, \tag{21}$$

with $Q_2' = (Q_2 + \frac{Q_3}{I\epsilon^2 - Mv_1^2})$. We are currently seeking a modulated solution of the following form:

$$\varphi_n = \varphi(t_1, t_2, x_1)e^{i(kna-\omega t)}. \tag{22}$$

The system is characterized by a slowly varying envelope that modulates a carrier wave, where $\varphi(t_1, t_2, x_1)$ is the relative excitation. The fast variable $(kna - \omega t)$, which represents the phase of the carrier wave, is treated as completely discrete. Additionally, x_1, t_1, and t_2 are classified as slow variables, also referred to as multitimescale variables, defined according to the relationships

$$t_0 = \epsilon^0 t, \quad t_1 = \epsilon^1 t, \quad t_2 = \epsilon^2 t,$$

and

$$x_1 = \epsilon na.$$

The derived operators associated are

$$\frac{\partial}{\partial t} = \frac{\partial}{\partial t} + \varepsilon\frac{\partial}{\partial t_1} + \varepsilon^2\frac{\partial}{\partial t_2},$$
$$\frac{\partial}{\partial x} = \varepsilon\frac{\partial}{\partial x_1}. \tag{23}$$

The substitution of Eq. (22) into Eq. (21), with the help of ϵ orders [82,84–86]

$$\varepsilon^0 : \omega = -2Q_1\cos(ka), \tag{24}$$

$$\varepsilon^1 : v_g = 2aQ_1\sin(ka), \tag{25}$$

$$\varepsilon^2 : i\frac{\partial\phi}{\partial t_2} + Q_2'|\phi|^2\phi + Q_1a^2\cos(ka)\frac{\partial^2\phi}{\partial x_1^2} = 0. \tag{26}$$

In Eq. (26) we introduce the impurities using an inhomogeneous mass of the form

$$M = m_0[1 + \Delta m\delta(x)]. \tag{27}$$

inserting Eq. (27) into Eq. (26), when taking the following variable $z = x_1 - v_g t_1$, $x = \epsilon x_1$, $t_2 = \epsilon^2 t$, and $\varphi = \frac{\Psi}{\epsilon}$, we generate the nonlinear Schrödinger equation (NSE) for charge transport in DNA in the presence of mass impurity:

$$i\frac{\partial\Psi}{\partial t} + P_1\frac{\partial^2\Psi}{\partial x^2} + P_2|\Psi|^2\Psi + \gamma\delta(x)\left[i\frac{\partial\Psi}{\partial t} + P_1\frac{\partial^2\Psi}{\partial x^2} + Q_2|\Psi|^2\Psi\right] = 0, \tag{28}$$

where $P_1 = -\frac{v_0}{\hbar}a^2\cos(ka)$, $\gamma = \frac{m_0v_1^2\Delta m}{I\epsilon^2 - m_0v_1^2}$, $Q_2 = \frac{(\alpha')^2}{\hbar K}$, and $P_2 = \frac{(2+2\cos(2k))K(\nu')^2\epsilon^2 - m_0v_1^2(\alpha')^2}{K\hbar(I\epsilon^2 - m_0v_1^2)}$.

B. Breather-type solutions in DNA

We generate the solution of Eq. (28) as follows:

For $\gamma = 0$ and $P_1P_2 > 0$, the latter admits bright breather-type soliton solutions of the following form [87]:

$$\Psi(x, t) = \mu\sqrt{2\frac{P_1}{P_2}}\,\text{sech}[\mu(x - x_0)]e^{iP_1\mu^2 t}, \tag{29}$$

with μ being a real positive parameter [84].

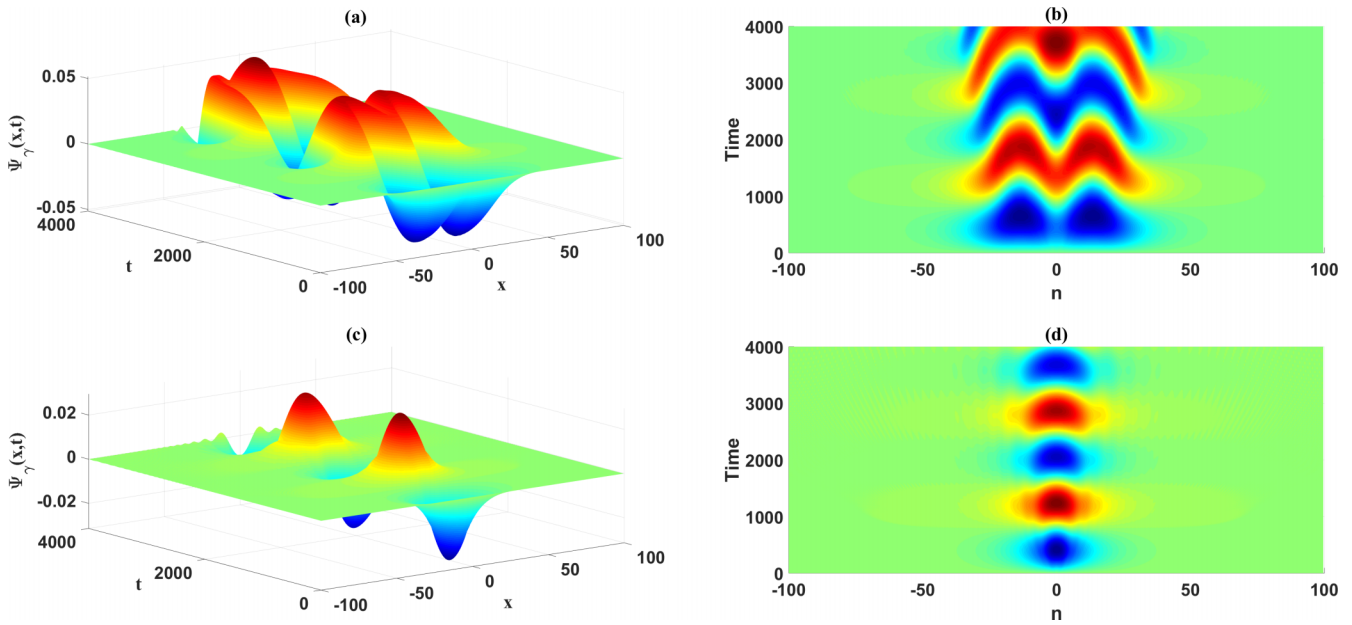


FIG. 7. Simulation of the localized impurity mode for different values of the mass impurity Δm for $\nu' = 0.04\,\text{eV Å}^{-1}$. (a,b) $\Delta m = -0.95$; (c,d) $\Delta m = 0.95$. The other parameters are $k = 0.45\pi$, $\alpha' = 0.13\,\text{eV Å}^{-1}$, $\nu^0 = 0.025\,\text{eV}$, $K = 0.855\,\text{eV Å}^{-2}$, $I = 0.062\,\text{eV Å}^{-2}$, $m_0 = 1$, $v_1 = 1.2$, $\delta_{0,0} = 1$, $\mu = 0.1$, and $a = 1$.

When $\gamma \neq 0$, we seek the impure mode solution of Eq. (28). Using the same approach as described in Sec. III of Ref. [82], the solution of Eq. (28) for the impure mode is of the form

$$\Psi_\gamma(x,t) = \theta_0 \text{sech}[\mu|x| + \tanh^{-1}(\gamma\theta_1)]e^{iP_1\mu^2 t}, \qquad (30)$$

with $\theta_0 = \mu\sqrt{2\frac{P_1}{P_2}}$, $\theta_1 = \frac{\mu}{2(1+\gamma)}$, and $\mu > \gamma$.

Figure 7 illustrates numerical simulations of the localized impurity mode in the Holstein-SSH model for two opposite values of the mass impurity Δm, namely, -0.95 [panels (a,b)] and $+0.95$ [panels (c,d)], using a weak effective coupling parameter($\nu' = 0.04\,\text{eV Å}^{-1}$) and fixed parameters such as $k = 0.45\pi$, $\alpha' = 0.13\,\text{eV Å}^{-1}$, $\nu^0 = 0.025\,\text{eV}$, $K = 0.855\,\text{eV Å}^{-2}$, $I = 0.062\,\text{eV Å}^{-2}$, basis mass $m_0 = 1$, velocity $v_1 = 1.2$, and $\mu = 0.1$. For negative Δm [panels (a,b)], corresponding to a light mass, the impure mode is strongly localized around the central site, with a clear maximum amplitude characteristic of a bright breather, indicating a strong charge trapping capacity. Furthermore, we note that, for a light mass, the charge density is slightly diffuse, with an amplitude less concentrated in the center but rather on neighboring sites, reflecting a tendency toward charge delocalization. On the other hand, for positive Δm [panels (c,d)], i.e., a heavier mass, the charge density is more stable, with an amplitude concentrated in the center of the network at the site $n = 0$, reflecting a local trapping capacity and a tendency toward charge localization.

These observations show that the impurity mass significantly controls the localization of energy and charge modes in the modeled DNA chain, which could directly influence the energy transport and dynamics of the system as predicted by the analysis in Fig. 5. The weakness of the ν' coupling reinforces the local character of these modes, highlighting the determining effect of the impurity mass in modulating the properties of these biological or nanotechnological systems.

Figure 8 evaluates the effect of ν^0 on the localized impurity mode. We note, just like in Fig. 7 described previously, that the impure mode remains strongly localized for negative Δm (-0.95) as shown in Figs. 8(a) and 8(b). On the other hand, the charge density remains concentrated around the central site $n = 0$ for positive Δm [Figs. 8(c) and 8(d)]. This situation is in agreement with the predictions of the analytical study of the MI through Fig. 4; meanwhile, for low values of ν^0, the system is slightly sensitive to impurities. On the other hand, high values of ν^0 strongly affect the dynamics of the system to impurities. This is well illustrated in Fig. 9.

Figure 9 provides a detailed analysis of the behavior of the localized impurity mode. It highlights the impact of the sign of the mass impurity Δm on the localization and shape of the charge modes. Simulations show that for negative Δm (-0.95) [Figs. 9(a) and 9(b)], the impure mode at $t = 0$ presents a high concentration around the impure site ($n = 0$), with a rapid decrease that reflects a very marked delocalization over time. This strong delocalization is accentuated by the high value of the transfer parameter $\nu^0 = 0.5\,\text{eV}$, which favors increased cohesion of the network while maintaining an intense concentration at the defect. This observed intense diffusion could be explained by the interaction between the charge transport dynamics and the disturbance induced by the impure mass, thus highlighting the sensitivity of the system to the coupling and mass parameters.

In contrast, when Δm is positive ($+0.95$) [Figs. 9(c) and 9(d)], the impure mode displays localization, but with a lower central amplitude and a smoother decay. This reflects a tendency toward less broad diffusion, where the positive mass acts as a barrier modifying the spatial distribution of the charge, making the mode more confined.

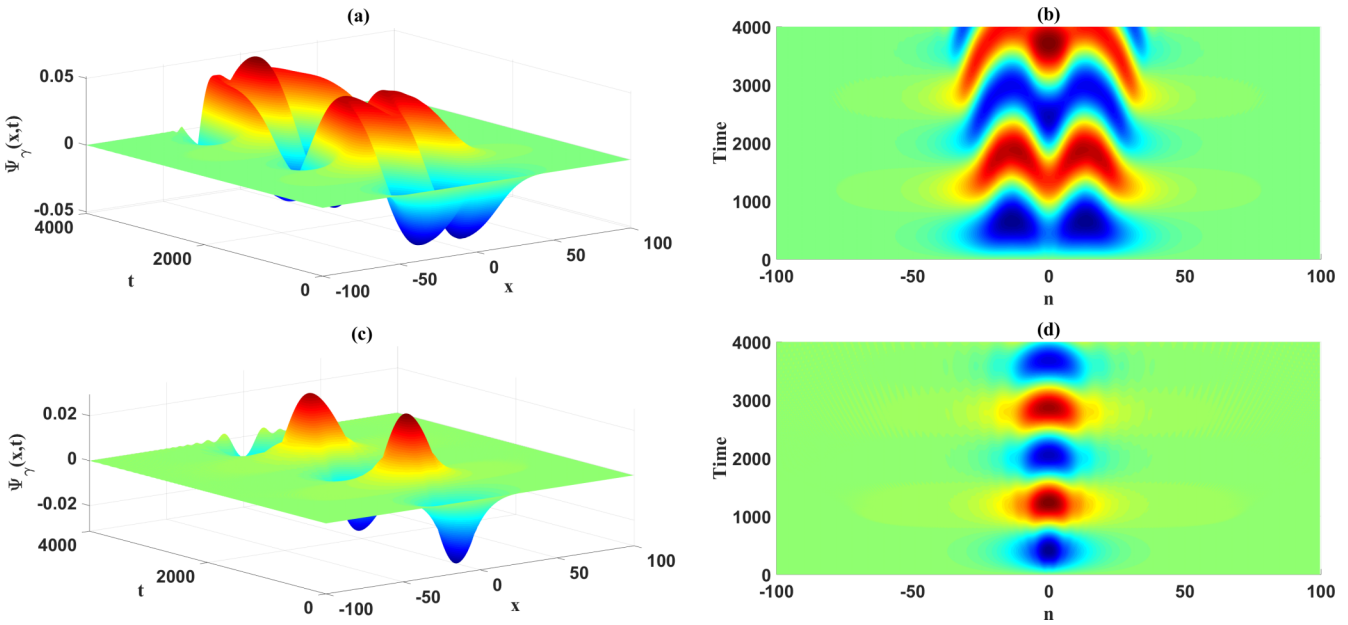


FIG. 8. Simulation of the localized impurity mode for different values of the mass impurity Δm for $\nu^0 = 0.025\,\text{eV}$. (a), (b) $\Delta m = -0.95$; (c), (d) $\Delta m = 0.95$. The other parameters are $k = 0.45\pi$, $\alpha' = 0.13\,\text{eV Å}^{-1}$, $\nu' = 0.04\,\text{eV Å}^{-1}$, $K = 0.855\,\text{eV Å}^{-2}$, $I = 0.062\,\text{eV Å}^{-2}$, $m_0 = 1$, $v_1 = 1.2$, $\delta_{0,0} = 1$, $\mu = 0.1$, and $a = 1$.

The notable difference between the profiles for negative and positive Δm illustrates the asymmetry induced by the nature of the impurity: a negative mass could function as a potential well, strongly capturing the charge locally, while a positive mass exerts a repulsive or dispersive effect. The high value of ν^0 amplifies these effects, reinforcing the network cohesion while modulating the mode localization. Thus, Figs. 7–9 highlight the crucial role of mass impurities in regulating charge transport, showing that their sign and amplitude can considerably influence the mode localization and shape, with potential implications for the design of biomolecular and nanotechnological devices where local control of electronic properties is essential. In nonlinear dynamics, a breather is a special type of nonlinear wave where energy is localized in space and oscillates in time.

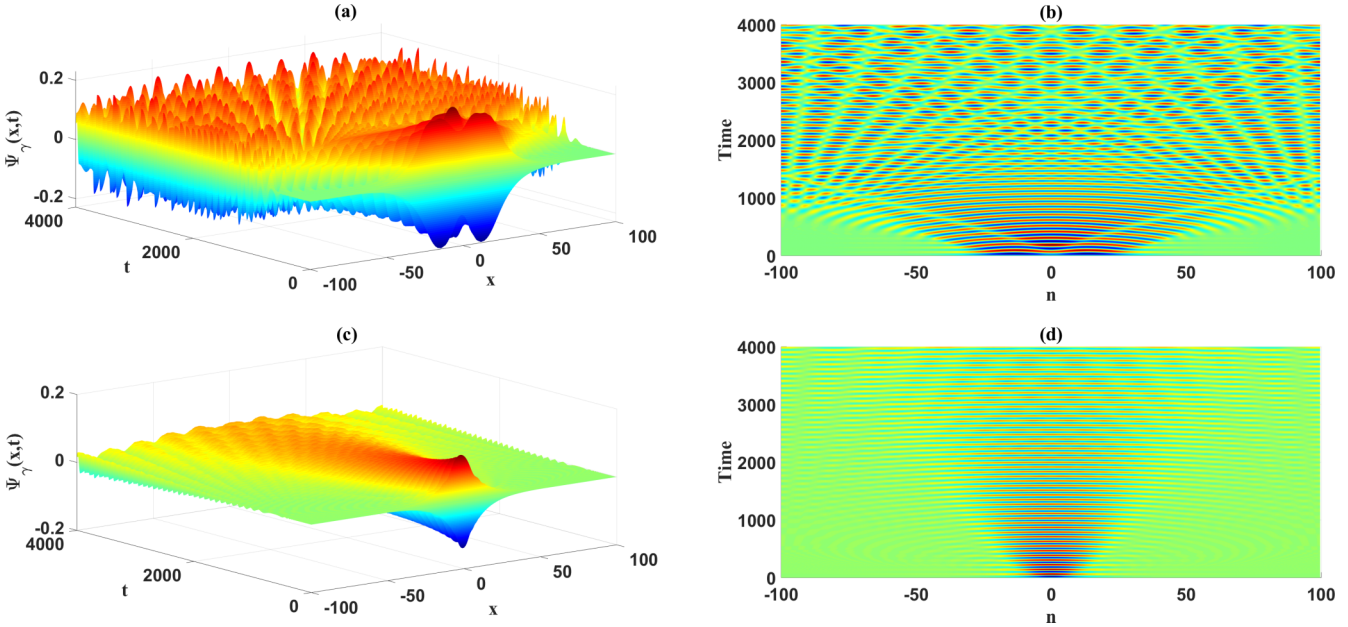


FIG. 9. Simulation of the localized impurity mode for different values of the mass impurity Δm for $\nu^0 = 0.5\,\text{eV}$. (a), (b) $\Delta m = -0.95$; (c), (d) $\Delta m = 0.95$. The other parameters are$k = 0.45\pi$, $\alpha' = 0.13\,\text{eV Å}^{-1}$, $\nu' = 0.04\,\text{eV Å}^{-1}$, $K = 0.855\,\text{eV Å}^{-2}$, $I = 0.062\,\text{eV Å}^{-2}$, $m_0 = 1$, $v_1 = 1.2$, $\delta_{0,0} = 1$, $\mu = 0.1$, and $a = 1$.

V. CONCLUSION

This study has provided insights into the stability of localized modes within a Holstein-SSH DNA model in the presence of a mass impurity. The system was modeled using a Hamiltonian that incorporates an inhomogeneous mass within a base pair. Using Hamilton's equations and the adiabatic approximation, we first derived a discrete nonlinear Schrödinger equation, followed by a semidiscrete version that describes charge transport in DNA with a mass impurity. A linear stability analysis based on the modulational instability (MI) phenomenon revealed that the evolution of the MI gain as a function of impurity parameters indicates that, for certain modes with wave numbers near the edge of the first Brillouin zone, the impurity mass m plays a more significant role in the dynamics of the carrier modes. We demonstrated that local modifications of the mass within a base pair act as a powerful regulator of charge wave stability. The effective coupling parameter, denoted as ν^0, influences the localization properties: low values reinforce the localized character of the modes, while higher values facilitate charge mobility between sites, making the system more susceptible to impurity effects. When ν^0 is high, charge transport becomes more delocalized, amplifying the impact of impurities and potentially destabilizing the propagation modes. To validate these analytical predictions, we conducted extensive numerical simulations. These confirmed that the impurity mass strongly controls the localization of energy and charge modes in the DNA chain, which can directly affect energy transport and system dynamics. Notably, the profiles differ significantly between negative and positive impurity masses, illustrating an asymmetry: a negative mass acts as a potential well, strongly trapping charge locally, whereas a positive mass exerts a repulsive or dispersive effect. Increasing the magnitude of the impurity mass enhances these effects, strengthening network cohesion while modulating mode localization. The strong agreement between analytical and numerical results emphasizes the critical role of mass impurities in regulating charge transport, demonstrating that their sign and amplitude can profoundly influence mode shape and localization.

Numerous previous studies, such as those by Ngoubi *et al.* [55,56] and Dang Koko *et al.* [58,59], have explored charge transport dynamics in DNA by analyzing the formation and propagation of localized nonlinear modes, leading to a better understanding of their stability in discrete or continuous models. However, our study is distinguished by the specific integration of a local mass impurity into a Holstein-SSH model, allowing us to more precisely analyze the impact of mass defects on mode stability and localization, particularly through modulational instability and breather formation. Our results confirm, like those of Ngoubi *et al.* [55,57], that breather formation is favored by the coupling effect. However, we further show that the nature of the mass defect (light or heavy) strongly influences the localization and stability of modes, a point little addressed in previous studies. For example, Dang Koko *et al.* [58] studied the propagation of localized modes without considering the impact of a mass impurity, which enriches our understanding by showing that these defects can act as traps or dispersives, modulating the formation and stability of local modes.

The charge localization profiles observed in our study, illustrating the formation of local modes (breathers) sensitive to impure mass, show similarities with other models, such as that of Ribama *et al.* [86]. Our analysis shows that impure mass, whether light or heavy, acts as a local potential: a light mass promotes localization by acting as a sink, while a heavy mass tends to disperse or displace the charge (Figs. 7–9). These results confirm that the nature of the defect strongly influences the stability and confinement of the charge, which is consistent with the literature on diffusion and trapping in chains with mass defects.

In summary, this study highlights the critical role that mass defects play in regulating the stability and localization of charge modes in biomolecular systems, with potential implications for the design of nanotechnological devices where precise control of electronic properties is essential.

The author contributions are as follows: R.Y.O.: design, conception, calculations, simulations, writing, reading, revision; A.D.K.: design, calculations, simulations, writing; R.A.A.R.: design, calculations, simulations, writing; C.B.T.: design, conception, reading, revision, and supervision; H.P.E.F.: design, conception, reading, revision, and supervision. J.P.N.: design, conception, reading, revision, and supervision.

The authors declare that they have no known competing financial interests or personal relationships that could have appeared to influence the work reported in this paper.

DATA AVAILABILITY

The data that support the findings of this article are not publicly available because they contain sensitive personal information. The data are available from the authors upon reasonable request.

[1] D. Tautz, Notes on the definition and nomenclature of tandemly repetitive DNA sequences, *DNA Fingerprinting: State of the Science* (1993), pp. 21–28.

[2] V. R. Harley, R. Lovell-Badge, and P. N. Goodfellow, Definition of a consensus DNA binding site for SRY, Nucleic Acids Res. **22**, 1500 (1994).

[3] L. Wang, W. Zhou, K. Wang, S. He, and Y. Chen, Predictive value of circulating plasma mitochondrial DNA for sepsis in the emergency department: Observational study based on the Sepsis-3 definition, BMC Emerg. Med. **20**, 25 (2020).

[4] A. W. Murray, How to compact DNA, Science **282**, 425 (1998).

[5] M. J. Puertas and M. González-Sánchez, Insertions of mitochondrial DNA into the nucleus—effects and role in cell evolution, Genome **63**, 365 (2020).

[6] D. M. Knipe, A. Prichard, S. Sharma, and J. Pogliano, Replication compartments of eukaryotic and bacterial DNA viruses:

Common themes between different domains of host cells, Annu. Rev. Virol. **9**, 307 (2022).
[7] R. Dwivedi, P. Prakash, B. V. Kumbhar, M. Balasubramaniam, and C. Dash, HIV-1 capsid and viral DNA integration, Mbio **15**, e00212 (2024).
[8] C. Chen, W. Wang, Z. Wang, F. Wei, and X. S. Zhao, Influence of secondary structure on kinetics and reaction mechanism of DNA hybridization, Nucleic Acids Res. **35**, 2875 (2007).
[9] A. Samanta, L. Baranda Pellejero, M. Masukawa, and A. Walther, DNA-empowered synthetic cells as minimalistic life forms, Nat. Rev. Chem. **8**, 454 (2024).
[10] P. J. Paukstelis and N. C. Seeman, 3D DNA crystals and nanotechnology, Crystals **6**, 97 (2016).
[11] A. Jaekel, P. Lill, S. Whitelam, and B. Saccà, Insights into the structure and energy of DNA Nanoassemblies, Molecules **25**, 5466 (2020).
[12] X. Yan, S. Huang, Y. Wang, Y. Tang, and Y. Tian, Bottom-up self-assembly based on DNA nanotechnology, Nanomaterials **10**, 2047 (2020).
[13] J. E. Deweese, M. A. Osheroff, and N. Osheroff, DNA topology and topoisomerases: Teaching a "knotty" subject, Biochem. Mol. Biol. Educ. **37**, 2 (2009).
[14] H. D. Ou, S. Phan, T. J. Deerinck, A. Inagaki, M. H. Ellisman, and C. C. O'Shea, ChromEMT: Visualizing and reconstructing chromatin ultrastructure and 3D organization in situ, Nat. Protoc. **20**, 934 (2025).
[15] J. Dekker and L. A. Mirny, The chromosome folding problem and how cells solve it, Cell **187**, 6424 (2024).
[16] A. Kuzminov, Bacterial nucleoid is a riddle wrapped in a mystery inside an enigma, J. Bacteriol. **206**, e00211 (2024).
[17] L. A. Loeb and K. C. Cheng, Errors in DNA synthesis: A source of spontaneous mutations, Mutat. Res. Rev. Genet. Toxicol. **238**, 297 (1990).
[18] Y. Kraytsberg, A. Nicholas, P. Caro, and K. Khrapko, Single molecule PCR in mtDNA mutational analysis: Genuine mutations vs. damage bypass-derived artifacts, Methods **46**, 269 (2008).
[19] A. Koren, P. Polak, J. Nemesh, J. J. Michaelson, J. Sebat, S. R. Sunyaev, and S. A. McCarroll, Differential relationship of DNA replication timing to different forms of human mutation and variation, Am. J. Hum. Genet. **91**, 1033 (2012).
[20] R. A. Bharat, S. P. Prathmesh, F. Sarsu, and P. Suprasanna, Induced mutagenesis using gamma rays: Biological features and applications in crop improvement, OBM Genet. **8**, 1 (2024).
[21] Y. Wang, C. Liu, C. Fang, Q. Peng, W. Qin, X. Yan, and K. Zhang, Engineered cancer nanovaccines: A new frontier in cancer therapy, Nano Micro Lett. **17**, 30 (2025).
[22] J. M. Gebicki and T. Nauser, Initiation and prevention of biological damage by radiation-generated protein radicals, Int. J. Mol. Sci. **23**, 396 (2021).
[23] P. Nurse, A long twentieth century of the cell cycle and beyond, Cell **100**, 71 (2000).
[24] P. K. Gupta, Single-molecule DNA sequencing technologies for future genomics research, Trends Biotechnol. **26**, 602 (2008).
[25] I. Pellarin, A. Dall'Acqua, A. Favero, I. Segatto, V. Rossi, N. Crestan, J. Karimbayli, B. Belletti, and G. Baldassarre, Cyclin-dependent protein kinases and cell cycle regulation in biology and disease, Signal Transduction Targeted Ther. **10**, 11 (2025).
[26] R. Mukhopadhyay, S. Nath, D. Kumar, N. Sahana, and S. Mandal, Basics of the molecular biology: From genes to its function, in *Genomics Data Analysis for Crop Improvement*, (Springer Nature, Singapore, 2024), p. 343.
[27] K. Numata and D. L. Kaplan, Silk proteins: Designs from nature with multipurpose utility and infinite future possibilities, Adv. Mater. **37**, 2411256 (2025).
[28] B. S. Chandana, S. A. Syed, S. J. Khanum, S. Abdurahman, M. N. Purohit, P. M. Vishwanath, and R. R. Achar, Structures and functions of biomolecules, *Biochemical and Molecular Pharmacology in Drug Discovery* (Elsevier, 2024), pp. 3–19.
[29] A. S. Giwa, N. Ali, and M. S. Akhter, Cellulose degradation enzymes in filamentous fungi, a bioprocessing approach towards biorefinery, Mol. Biotechnol. **67**, 2931 (2025).
[30] M. M. Goodarzi and R. Jalalirad, Clear insight into complex multimodal resins and impurities to overcome recombinant protein purification challenges: A review, Biotechnol. Bioeng. **122**, 5 (2025).
[31] J. Briggs and P. R. Panfili, Quantitation of DNA and protein impurities in biopharmaceuticals, Anal. Chem. **63**, 850 (1991).
[32] R. Nian and P. Gagnon, Advance chromatin extraction enhances performance and productivity of cation exchange chromatography-based capture of immunoglobulin G monoclonal antibodies, J. Chromatogr. A **1453**, 54 (2016).
[33] C. Courts, A. Gosch, and M. Rothschild, RNA analysis in forensic molecular biology, Dtsch. Aerztebl. Int. **121**, 363 (2024).
[34] S. C. Tan and B. C. Yiap, DNA, RNA, and protein extraction: The past and the present, Biomed Res. Int. **2009**, 574398 (2009).
[35] M. B. S. Al-Shuhaib and H. O. Hashim, Mastering DNA chromatogram analysis in Sanger sequencing for reliable clinical analysis, J. Genet. Eng. Biotechnol. **21**, 115 (2023).
[36] A. Shirizadeh, M. Ebrahimpur, S. Soltani, and G. Solgi, Chemical contamination in the extracted DNA affects the results of HLA typing by the PCR-SSOP method, Mol. Biol. Rep. **52**, 23 (2025).
[37] G. Lucena-Aguilar, A. M. Sánchez-López, C. Barberán-Aceituno, J. A. Carrillo-Ávila, J. A. López-Guerrero, and R. Aguilar-Quesada, DNA source selection for downstream applications based on DNA quality indicators analysis, Biopreserv. biobanking **14**, 264 (2016).
[38] A. E. Basyoni, A. Atta, M. M. Salem, and T. M. Mohamed, Harnessing exosomes for targeted drug delivery systems to combat brain cancer, Cancer Cell Int. **25**, 150 (2025).
[39] A. R. Arnold, M. A. Grodick, and J. K. Barton, DNA charge transport: From chemical principles to the cell, Cell chem. biol. **23**, 183 (2016).
[40] K. Klepárník and P. Boček, Electrophoresis today and tomorrow: Helping biologists' dreams come true, BioEssays **32**, 218 (2010).
[41] K. S. Kwok and J. C. Ellenbogen, Moletronics: Future electronics, Mater. Today **5**(2), 28 (2002).
[42] D. D. Eley and D. I. Spivey, Semiconductivity of organic substances. Part 9.—Nucleic acid in the dry state, Trans. Faraday Soc. **58**, 411 (1962).
[43] H. W. Fink and C. Schönenberger, Electrical conduction through DNA molecules, Nature (London) **398**, 407 (1999).
[44] N. Rizan, T. Y. Shin, H. A. Tajuddin, G. Gnana kumar, and V. Periasamy, Effect of pH on the conductivity of basidiomycetes DNAs integrated within Schottky-like junctions, ChemistrySelect **5**, 601 (2020).

[45] Y. Wang, Y. Xie, M. Gao, W. Zhang, L. Liu, Y. Qu, J. Wang, C. Hu, Z. Song, and Z. Wang, Electrical conductivity measurement of λ DNA molecules by conductive atomic force microscopy, Nanotechnology **33**, 055301 (2022).

[46] N. Gupta, D. Kumar, A. Das, S. Sood, and B. D. Malhotra, Conductive ink-coated paper-based supersandwich DNA biosensor for ultrasensitive detection of *Neisseria gonorrhoeae*, Biosensors **13**, 486 (2023).

[47] R. Di Felice, A. Calzolari, and H. Zhang, Towards metalated DNA-based structures, Nanotechnology **15**, 1256 (2004).

[48] H. Yamada and K. Iguchi, Some effective tight-binding models for electrons in DNA conduction: A review, Adv. Condens. Matter Phys. **2010**, 380710 (2010).

[49] A. Bende, F. Bogár, and J. Ladik, Model calculations of the energy band structures of double stranded DNA in the presence of water and Na ions, Solid State Commun. **151**, 301 (2011).

[50] S. Sun, Y. Zhang, X. Shi, W. Sun, C. Felser, W. Li, and G. Li, From charge to spin: An in-depth exploration of electron transfer in energy electrocatalysis, Adv. Mater. **36**, 2312524 (2024).

[51] R. Goobes, O. Cohen, and A. Minsky, Unique condensation patterns of triplex DNA: Physical aspects and physiological implications, Nucleic Acids Res. **30**, 2154 (2002).

[52] P. Mandrekar and A. Mandal, Pathogenesis of alcohol-associated liver disease, Clin. Liver Dis. **28**, 647 (2024).

[53] D. Hennig, J. F. Archilla, and J. Agarwal, Nonlinear charge transport mechanism in periodic and disordered DNA, Physica D **180**, 256 (2003).

[54] C. B. Tabi, A. Mohamadou, and T. C. Kofané, Modulational instability of charge transport in the Peyrard–Bishop–Holstein model, J. Phys.: Condens. Matter **21**, 335101 (2009).

[55] H. Ngoubi, G. H. Ben-Bolie, and T. C. Kofané, Charge transport in a DNA model with solvent interaction, J. Biol. Phys. **44**, 483 (2018).

[56] H. Ngoubi, G. H. Ben-Bolie, and T. C. Kofané, Delocalized charge through the DNA with microscopic effect, Eur. Phys. J. Plus **137**, 166 (2022).

[57] H. Ngoubi, I. Sali, A. Mvogo, G. H. Ben-Bolie, and T. C. Kofané, Multi-exciton transfer in a biomolecular system, Nonlinear Dyn. **112**, 3887 (2024).

[58] A. Dang Koko, C. B. Tabi, H. P. Ekobena Fouda, and T. C. Kofané, Discrete charge patterns in a Holstein-SSH DNA lattice, Int. J. Quantum Chem. **115**, 34 (2015).

[59] D. Belobo Belobo and A. Dang Koko, Bright solitary waves as charge transport in DNA: A variational approximation, Biopolymers **111**, e23346 (2020).

[60] S. M. Rayhanul Islam, S. M. Yiasir Arafat, and M. Inc, Exploring novel optical soliton solutions for the stochastic chiral nonlinear Schrödinger equation: Stability analysis and impact of parameters, J. Nonlinear Opt. Phys. Mater. **34**, 2450009 (2025).

[61] U. Younas, J. Muhammad, H. F. Ismael, M. A. S. Murad, and T. A. Sulaiman, Optical fractional solitonic structures to decoupled nonlinear Schrödinger equation arising in dual-core optical fibers, Mod. Phys. Lett. B **39**, 2450378 (2025).

[62] S. Abbagari, A. Houwe, L. Akinyemi, and S. Y. Doka, Soliton interaction and nonlinear localized waves in one-dimensional nonlinear acoustic metamaterials, Physica D **476**, 134591 (2025).

[63] D. Mahmoud, S. Abdoulkary, L. Q. English, and A. Mohamadou, Propagation of acoustic solitons in a nonlinear left-handed transmission line, Wave Motion **139** 103597 (2025).

[64] E. M. Zayed, B. M. Saad, A. H. Arnous, and Y. Yildirim, Novel solitary wave solutions in a generalized derivative nonlinear Schrödinger equation with multiplicative white noise effects, Nonlinear Dyn. **113**, 7139 (2025).

[65] D. Chou, H. U. Rehman, A. Amer, and M. S. Osman, Optical soliton dynamics of the conformable nonlinear evolution equation in Bose-Einstein condensates, Rend. Lincei. Sci. Fis. Nat. **35**, 1065 (2024).

[66] M. M. Khater, S. H. Alfalqi, and A. Vokhmintsev, Dynamic behavior of solitons in nonlinear Schrödinger equations, Sci. Rep. **15**, 4101 (2025).

[67] D. Chevizovich, D. Michieletto, A. Mvogo, F. Zakiryanov, and S. Zdravković, A review on nonlinear DNA physics, R. Soc. Open Sci. **7**, 200774 (2020).

[68] A. Zafar, K. K. Ali, M. Raheel, N. Jafar, and K. S. Nisar, Soliton solutions to the DNA Peyrard–Bishop equation with beta-derivative via three distinctive approaches, Eur. Phys. J. Plus **135**, 726 (2020).

[69] T. Shafique, M. Abbas, A. Mahmood, F. A. Abdullah, A. S. Alzaidi, and T. Nazir, Solitary wave solutions of the fractional Peyrard Bishop DNA model, Opt. Quantum Electron. **56**, 815 (2024).

[70] S. Nawaz, M. O. Ahmed, M. Z. Baber, E. Bittaye, and M. W. Yasin, Explicit solitary wave structure for the stochastic resonance nonlinear Schrödinger equation under Brownian motion with dynamical analysis, Sci. Rep. **15**, 31817 (2025).

[71] E. M. Boon and J. K. Barton, Charge transport in DNA, Curr. Opin. Struct. Biol. **12**, 320 (2002).

[72] D. W. Kang, J. H. You, and L. B. Li, The effect of hydrogen bond breaking defect on charge transport in a DNA molecular device, Physica B **407**, 184 (2012).

[73] A. Alvarez, F. R. Romero, J. F. R. Archilla, J. Cuevas, and P. V. Larsen, Breather trapping and breather transmission in a DNA model with an interface, Eur. Phys. J. B **51**, 119 (2006).

[74] C. L. Gninzanlong, F. T. Ndjomatchoua, and C. Tchawoua, Forward and backward propagating breathers in a DNA model with dipole-dipole long-range interactions, Phys. Rev. E **102**, 052212 (2020).

[75] S. Flach and K. Kladko, Moving discrete breathers? Physica D **127**, 61 (1999).

[76] J. F. Zhao, S. Zhou, X. F. Fang, and H. Zhang, Managment of nonautonomous breather molecules and rogue waves in plasma physics, Chaos, Solitons Fract. **195**, 116277 (2025).

[77] R. A. A. Ribama, M. Youssoufa, R. Y. Ondoua, Z. I. Djoufack, and J. P. Nguenang, Influence of next-nearest neighbor interactions on the dynamics of discrete energy transport within neuronal microtubules, Chaos, Solitons Fract. **198**, 116538 (2025).

[78] F. Schindler, V. B. Bulchandani, and W. A. Benalcazar, Nonlinear breathers with crystalline symmetries, Phys. Rev. B **111**, 064312 (2025).

[79] J. Cuevas, F. Palmero, J. F. R. Archilla, and F. R. Romeo, Moving discrete breathers in Klein-Gordon chain with impurity, J. Phys A: Math. Gen. **35**, 10519 (2002).

[80] R. Y. Ondoua and D. Belobo Belobo, Solitary waves dynamic for Davydov α-helical protein model: Effects of localized and periodic inhomogeneities, Phys. Rev. E **102**, 062414 (2020).

[81] R. Y. Ondoua, C. B. Tabi, H. P. Ekobena, A. Mohamadou, and T. C. Kofané, Discrete energy transport in the perturbed Ablowitz-Ladik equation for Davydov model of α-helix proteins, Eur. Phys. J. B **85**, 318 (2012).

[82] Z. I. Djoufack, R. Abouem A Ribama, and J. P. Nguenang, Impurity-impurity and impurity- breather interactions combined with energy localization in a quantum 1D Klein-Gordon chain, Chaos, Solitons Fract. **168**, 113208 (2023).

[83] M. Youssoufa, O. Dafounansou, M. Inc, S. Rezapour, Alim, and A. Mohamadou, Traveling waves, chaos and solitons in a cubic-quintic nonlinear optical media, Comput. Appl. Math. **44**, 119 (2025).

[84] L. Yang and T. Yi, Bright and dark small amplitude nonlinear localized modes in a quantum one-dimensional Klein–Gordon chain, Chin. Phys. B **17**, 3841 (2008).

[85] R. A. A. Ribama, Z. I. Djoufack, and J. P. Nguenang, Breather-impurity interactions and modulational instability in a quantum 2D Klein–Gordon chain, Eur. Phys. J. B **95**, 86 (2022).

[86] R. Abouem A Ribama, Z. I. Djoufack, and J. P. Nguenang, Scattering of impure mode and self-trapping phenomenon in a 1D quantum diatomic Klein–Gordon chain containing a mass defect, Eur. Phys. J. Plus **139**, 193 (2024).

[87] R. Abouem A Ribama, Z. I. Djoufack, and J. P. Nguenang, Effects of nonlinear coupling parameters on the formation of intrinsic localized modes in a quantum 1D mixed Klein-Gordon/Fermi-Pasta-Ulam chain, Physica D **473**, 134556 (2025).